Visualising bifurcations in high dimensional systems: The spectral bifurcation diagram

David Orrell[1] and Leonard A. Smith[2,3]

[1] Institute for Systems Biology, 1441 N 34th Street, Seattle, WA 98103, USA
[2] Mathematical Institute, University of Oxford, 24-29 St Giles', Oxford OX1 3LB, UK
[3] Centre for the Analysis of Time Series, Department of Statistics, London School of Economics, Houghton Street, London WC2A 2AE, UK

Manuscript submitted to

IJBC

Manuscript version from February 28, 2003

Abstract

Bifurcation diagrams which allow one to visualise changes in the behaviour of low dimensional nonlinear maps as a parameter is altered are common. Visualisation in higher dimensional systems is more difficult. A straightforward method to visualise bifurcations in flows of high dimensional nonlinear dynamical systems is presented, using the Lorenz '96 systems with dimension 8 and dimension 40 as examples. Three techniques are considered; the first two, density and max/min diagrams, are analogous to the traditional bifurcation diagrams used for maps. These diagrams are generally more difficult to interpret than the corresponding diagrams of maps, however, due to projection effects and the continuous nature of the flow. The third technique introduces an alternative approach: by calculating the power spectrum at each value of the control parameter, a plot is produced which clearly shows the changes between periodic, quasi-periodic, and chaotic states; these spectral bifurcation diagrams reveal structure not shown by the other methods.

1 Introduction

Bifurcation diagrams provide a useful method to show how a system's behaviour changes according to the value of a control parameter. A classic example is the logistic map, where the system shows both periodic and chaotic behaviour, and periodic orbits appear as a discrete set of points [Alligood *et al.*, 1996]. With flows, it is more difficult to present the bifurcations, due to the continuous nature of the flow. While a periodic orbit in a map is an oscillation between a discrete number of points, in a flow a variable will sweep out a continuous range of values. In this paper, we discuss different methods for visualising bifurcations in flows, and present a new technique based on calculating the power spectrum. The techniques are illustrated using the Lorenz '96 systems, though they can also be applied to other systems. The emphasis is on visualising the bifurcations, rather than exploring their nature using other means, which is a topic for future work.

The Lorenz '96 systems were first introduced as idealised one-dimensional models of the atmosphere [Lorenz, 1996]. They produce time series which are qualitatively similar to the behavior of variables such as temperature. Variants of the systems have proved useful for studying issues related to atmospheric predictability and model error [Hansen, 1998; Hansen & Smith, 2000; Orrell *et al.*, 2001; Orrell, 2002].

The first system, which we shall refer to as System I, contains n variables $x_1, x_2, ..., x_n$, and the equations are

$$\frac{dx_i}{dt} = x_{i-1}(x_{i+1} - x_{i-2}) - x_i + F, \quad \text{i=1,...,n} \tag{1}$$

where F is a constant, and the index i is cyclic so that $x_{i-n} = x_{i+n} = x_i$. The x_i's can therefore be viewed as variables around a circle. In physical terms, they could be values of some atmospheric quantity such as temperature at n equally spaced latitudes around the globe. The constant term F

in the equations is external forcing, the linear term is internal damping, and the quadratic terms, which introduce information about the spatial variation of x, represent advection.

The other system to be discussed will be referred to as System II, and incorporates smaller scale motions with shorter time scales. There are n variables $\tilde{x}_i$, together with an additional nm variables $\tilde{y}_{i,j}$. The equations are

$$\begin{aligned} \frac{d\tilde{x}_i}{dt} &= \tilde{x}_{i-1}(\tilde{x}_{i+1} - \tilde{x}_{i-2}) - \tilde{x}_i + F - \frac{hc}{b}\sum_{j=1}^{m} \tilde{y}_{i,j} \\ \frac{d\tilde{y}_{i,j}}{dt} &= cb\tilde{y}_{i,j+1}(\tilde{y}_{i,j-1} - \tilde{y}_{i,j+2}) - c\tilde{y}_{i,j} + \frac{hc}{b}\tilde{x}_i \end{aligned} \tag{2}$$

for $i = 1, \ldots, n$ and $j = 1, \ldots, m$. Again the variables are cyclic so that $\tilde{y}_{i+n,j} = \tilde{y}_{i,j}$ and $\tilde{y}_{i,j-m} = \tilde{y}_{i-1,j}$. Following [Lorenz, 1996], we set $b = c = 10$, which has the effect of making the $\tilde{y}$'s fluctuate ten times more rapidly than the $\tilde{x}$'s. The $\tilde{y}$'s can be thought of as convective scale quantities in the atmospheric analogy. The coupling coefficient h is set (except when otherwise specified) to 1.

2 Behaviour of System I with dimension 4

We begin by considering System I with $n = 4$, which is the simplest non-trivial variant. We first derive some of the basic properties of the system, before presenting the bifurcation behaviour. The equations are:

$$\begin{aligned} \frac{dx_1}{dt} &= x_4(x_2 - x_3) - x_1 + F \\ \frac{dx_2}{dt} &= x_1(x_3 - x_4) - x_2 + F \\ \frac{dx_3}{dt} &= x_2(x_4 - x_1) - x_3 + F \\ \frac{dx_4}{dt} &= x_3(x_1 - x_2) - x_4 + F \end{aligned} \tag{3}$$

By substituting into the equations, it is easily seen that $x_1 = x_2 = x_3 = x_4 = F$ is a fixed point for all F. The stability of this fixed point can be determined by considering the Jacobean [Guckenheimer & Holmes, 1983], which is:

$$\begin{pmatrix} -1 & x_4 & -x_4 & x_2 - x_3 \\ x_3 - x_4 & -1 & x_1 & -x_1 \\ -x_2 & x_4 - x_1 & -1 & x_2 \\ x_3 & -x_3 & x_1 - x_2 & -1 \end{pmatrix}$$

For $F = 0$, the Jacobean evaluated at the origin $(x_1 = x_2 = x_3 = x_4 = 0)$ is minus the identity, thus the only eigenvalue is -1 which ensures stability. For $F = 1$, the Jacobean at the fixed point $x_1 = x_2 = x_3 = x_4 = 1$ is

$$\begin{pmatrix} -1 & 1 & -1 & 0 \\ 0 & -1 & 1 & -1 \\ -1 & 0 & -1 & 1 \\ 1 & -1 & 0 & -1 \end{pmatrix}$$

An eigenvector of this matrix is (i,-1, $-i$, 1), with associated eigenvalue i. At $F = 1$ an eigenvalue passes through the real axis in the complex plane. This is associated with a Hopf bifurcation [Guckenheimer & Holmes, 1983], where a periodic orbit is produced from a fixed point. Indeed, in Figure 1 we see that for F just above 1, the system attractor plotted as x_1 versus x_2 is a near circular stable periodic orbit with period of approximately 2π. The variables x_2, x_3 and x_4 (not shown) also follow periodic orbits but are out of phase with x_1 by $\pi/2$, π and $3\pi/2$ respectively. Viewed as variables on a circle, the solution can then be seen as a wave propagating in a clockwise direction. This direction of propagation remains noticeable even when the system is chaotic, and is a consequence of the advection term. The power spectrum of the time series of x_1 shows a peak

at frequency $1/2\pi$, as expected, but also reveals a number of higher harmonics at multiples of the base frequency.

As F is increased, the x_1 time series picks up extra local maxima due to the presence of higher harmonics, but there is no sign of period doubling. In the logarithmic scale, the power appears to decrease more or less linearly with frequency, suggesting that the coefficients in the power spectrum decrease exponentially with frequency. Near $F = 12$, the system becomes chaotic. Around $F = 14.7$ there is a periodic window before becoming chaotic again. The orbit shown in the lower panels has a period of 11.365 time units.

Rather than examining individual values of F, it is desirable to visualize how the system changes, and particularly where bifurcations occur, as F is varied continuously. One method to do this is analogous to the bifurcation diagrams of maps such as the logistic map, which simply record the points on the attractor as the bifurcation parameter is increased, either by a scatter plot or a density plot. For example, the top panel of Figure 2 shows a density plot of the x_1 variable (again, by symmetry, it doesn't matter which x_i is chosen). For each value of F, it records the density of the x_1 time series, of the sort shown in the left column of Figure 1.

While the resulting diagram is interesting and captures much of the behavior, a disadvantage of the method, which doesn't occur with maps, is that because x_1 is a continuous variable, the periodic orbits appear as a continuous band rather than discrete points, and it is hard to distinguish areas of chaos. This can be improved by showing only local minima or maxima. A period p orbit produces a finite number of local maxima, while in a chaotic region, we expect an infinite number of such maxima. This method is used in the max/min figure in the middle panel; it is again a density plot, but now only shows the local extrema of x_1 (either local maximum or local minimum). Interpreting this graph, the line which appears at $F = 1$ represents the nearly linear

growth in the frequency of the solution as F is increased. The new lines which appear around $F = 3$ and $F = 8$ (and higher values of F) reflect the higher harmonics (note that these lines do not indicate period doubling). The system becomes chaotic around $F = 12$, and the periodic window at $F = 14.7$, as well as a second window just before $F = 16$, can be clearly seen.

While these diagrams give useful information, new lines representing the growth of higher harmonics appear out of nowhere, and needn't indicate any bifurcation. Because the system picks up progressively higher harmonics as F increases, the more natural approach is the *spectral bifurcation diagram* in the lower panel. This new kind of bifurcation diagram was inspired by a technique used to do on-the-fly measurements of field harmonics in superconducting magnets [Orrell *et al.*, 1994] while the current is being ramped. The diagram is composed by combining the power spectra at different values of F into a continuous power histogram. The vertical axis shows frequency, while the color indicates the power at that frequency.

Comparing the spectral bifurcation diagram with Figures 1 and the upper two panels, we see that the lines beginning at and after $F = 1$ and continuing to $F = 12$ represent the periodic orbits. These lines are equally spaced in frequency, indicating that the orbit in this region of parameter space only contains harmonics which are multiples of its lowest frequency (this ensures periodicity). Around $F = 12$ the chaotic regime begins. The periodic windows, such as the one near $F = 16$, appear as bands of horizontal lines. The period of the orbit at $F = 14.7$ may be estimated from its lowest frequency of about 0.88, which agrees with the observed period 11.365.

The main advantage of the spectral bifurcation diagram is that it can reveal structure, such as quasi-periodic orbits, which are not seen using the other methods. This is evident in the next section, where we consider higher-dimensional systems.

3 System I with dimension 8 and 40

System I can be run with any number of variables. While the higher dimension versions display broadly similar behaviour to the 4D case, they also show additional complications and interesting features. One property of the $n = 8$ system is that it has at least two attractors: a symmetric attractor $(x_5 = x_1, x_6 = x_2, x_7 = x_3, x_8 = x_4)$ which is a copy of the $n = 4$ attractor, and a second attractor containing no such points. This symmetric attractor will attract any initial condition which has the required symmetry, while other points are drawn to the other attractor [Hansen, 1998]. Therefore periodic orbits corresponding to those in Figure 1, even the one at $F = 14.7$ where most orbits are strongly chaotic, all exist in the $n = 8$ system. The analysis below is concerned with the second (asymmetric) attractor.

Figure 3 shows bifurcation diagrams for the $n = 8$ case. They are similar to the attractor for the $n = 4$ system, but become chaotic much earlier. Prior to about $F = 2.8$, the attractors for $n = 4$ and $n = 8$ correspond, in the sense that trajectories in the $n = 8$ system are drawn to the symmetric periodic orbits. However around $F = 2.8$ a period-doubling bifurcation occurs, as shown in Figure 4, and we will no longer have $x_1 = x_5$ and so on. By $F = 3.8$, the system appears to be chaotic. At this resolution, it is difficult to pick out periodic windows of any width in the chaotic regime past $F = 4.5$.

The spectral bifurcation diagram in the lower panel of Figure 3 reveals completely new features that are not evident from the density and max/min diagrams. The symmetric periodic orbit is indicated by the line beginning at $F = 1$ and frequency 0.16. At $F = 2.8$ a line appears at half the frequency, which corresponds to the period doubling mentioned above. By $F = 4$ we see a broad range of harmonics corresponding to chaos. However from about $F = 4.8$ to $F = 5.6$ there are large windows where the system appears not to be chaotic (specifically, it is not broad band).

Inspection of the spectral bifurcation diagram reveals that more than one frequency, or its harmonics, are present in these windows. The slopes of the diagonal lines in the range $F = 4.8$ to $F = 5.6$ are different, so the relative balance of power between the frequencies changes with F. When the frequencies are incommensurate, the result will be a quasi-periodic orbit. In bifurcation diagrams produced either by the maxima method or a Poincaré section method [Alligood *et al.*, 1996], these quasi-periodic orbits appear as a continuous band indistinguishable from chaos.

It is possible to find orbits in the region $F = 4.8$ to $F = 5.6$ which appear to close upon themselves (that is, the attractor is a periodic orbit); this is shown in Figure 5 for $F = 5.235298$. The number of decimal places in F, however, attests to the fact that this is not an easy task! The period of this orbit is 36.7, which corresponds to a frequency of 0.027. Figure 6 is a close-up of the spectral bifurcation diagram. The periodic orbit is located in a region where the spectra display lines separated with a frequency spacing of 0.027, as expected.

Still another way to view, or experience, the bifurcations is to listen to them [Orrell, 2001]. A recording is available[1] which contains a translation of the 8 dimension system into sound. The x_1 and x_5 variables are interpreted as sound waves, and played to the left and right speakers respectively. Starting from a periodic orbit at $F = 3.5$, the system is ramped upwards. The periodic orbit increases in speed and sound level, like a motor being accelerated. A distinct change is heard as the system goes chaotic around $F = 3.8$; the sound level drops and becomes irregular, as if the motor is about to stall. Entering the quasi-periodic region around $F = 4.7$, the system once again settles down, though it doesn't quite repeat. Only when held at a value of $F = 5.235298$ is a true rhythm established. It seems that the Lorenz systems provide a model of a car in need of a tune as well as the atmosphere!

[1] At www.lse.ac.uk/collections/cats/documents.htm

The dimension of the system can be increased indefinitely, but computations rapidly become expensive. The highest dimension we considered was $n = 40$. Figure 7 shows bifurcations for the 40D System I. It is again quite similar to the other systems, with the exception that the spectral bifurcation diagram (lower panel) has a somewhat richer appearance in the transition to chaos.

The systems considered so far have all had a constant forcing term F. Other variants are possible; one studied is the case where F depends on the index i. This is analogous to the weather problem where forcing is different over land and over sea [Hansen, 1998; Hansen & Smith, 2000]. Other possibilities include making the forcing function a function of space and time (seasonal forcing), or a function of the local value of x_i, or all values of x_i at the current time, or values of x_i at current and previous times, and so on. System II may be considered as one such variant, where the forcing depends on small scale $\tilde{y}$ variables which are coupled with the large scale $\tilde{x}$ variables.

4 Behaviour of System II

The equations for the $\tilde{x}$ variables in System II are similar to those of System I, with the difference that the constant forcing is replaced by a term which depends on the fast scale $\tilde{y}$ variables. We might therefore expect the $\tilde{x}$ variables to behave like the x's in System I, but with an added degree of fuzziness. The density and max/min bifurcation diagrams for the $n = 8, m = 4$ case (dimension 40) in Figure 8 bear this out. They are qualitatively quite similar to Figure 3. The lines in the region $F = 4$ to $F = 5$ have an added thickness, and correspond to apparently chaotic orbits that are like jostled versions of the periodic orbits seen in System I for slightly lower values of F. There is an additional period doubling bifurcation at $F = 1.5$, as the fast scale variables become non-zero. Another noticeable feature is that the $\tilde{y}$ variables tend to decrease the forcing F on average, so the

whole diagram is shifted to the right compared to Figure 3.

The spectral bifurcation diagram for System II in Figure 8 can be compared also with that in Figure 3. Again it is quite similar to the System I case, with the difference that a full range of spectra, indicating a completely chaotic regime, doesn't occur until around $F = 5.5$ as opposed to $F = 4$. The diagram only shows to $F = 6$, however the system appears to remain chaotic and there no obvious periodic or quasi-periodic windows visible past that point. Figure 9 shows bifurcation diagrams for the $\tilde{y}$ variables.

So far we have only considered bifurcations obtained by varying the parameter F. There are of course other possibilities, such as varying the coefficient h, which controls the coupling between the small scale $\tilde{y}$ variables and the large scale $\tilde{x}$ variables. Figure 10 shows bifurcations in the $\tilde{y}$ variables as the coefficient h is varied, while the forcing is held constant at $F = 2$. The spectral bifurcation diagram shows intricate cross-hatching, and a degree of structure that is absent from the other diagrams.

When the coupling coefficient is increased, System II is capable of showing quite complicated behaviour even at $F = 2$, where System I is periodic. Figure 11 shows the $\tilde{x}$ and $\tilde{y}$ orbits. The $\tilde{x}$ variables nearly follow a periodic orbit, while the $\tilde{y}$ variables are clearly quasi-periodic.

5 Conclusions and future work

In this paper, we have discussed different methods for viewing bifurcations in high dimensional nonlinear dynamical flows. The most useful, in terms of the amount of information conveyed, is the spectral bifurcation diagram. These diagrams reveal a sometimes surprising amount of detail in system behaviour which would not otherwise be evident.

The methods have been illustrated throughout using the Lorenz '96 systems. While these sys-

tems are useful for simulating certain properties of atmospheric models, they also turn out to be interesting in their own right. Spectral bifurcation diagrams reveal the extraordinarily rich structure of their bifurcations.

While this paper has concentrated on techniques for visual presentation of bifurcations, it would clearly be interesting to explore the nature of the Lorenz '96 bifurcations in greater detail. We hope that the results here will serve as motivation for such work.

Acknowledgements. Thanks to J. Hansen, I. Gilmour and S. Bishop for many discussions. This work was supported by ONR DRI Grant N00014-99-1-0056; DO was partially supported by an EPSRC CASE studentship with the European Centre for Medium-Range Weather Forecasts.

References

Alligood, K.T., Sauer, T.D. & Yorke, J.A. [1996] *Chaos: An Introduction to Nonlinear Dynamical Systems*, (Springer-Verlag, NY).

Guckenheimer, J. & Holmes, P. [1983] *Nonlinear Oscillations, Dynamical Systems, and Bifurcations of Vector Fields*, (Springer-Verlag, NY).

Hansen, J. A. [1998] "Adaptive Observations in Spatially-extended, Nonlinear Dynamical Systems," D.Phil. thesis, Oxford University.

Hansen, J.A. & Smith, L.A. [2000] "The Role of Operational Constraints in Selecting Supplementary Observations," *J. Atmos. Sci.* **57**, 2859-2871.

Lorenz, E. [1996] "Predictability - a problem partly solved," in *Predictability*, edited by T. Palmer, European Centre for Medium-Range Weather Forecasting, Shinfield Park, Reading, UK.

Orrell, D. [2001] "Modelling nonlinear dynamical systems: chaos, error and uncertainty," *D.Phil. thesis, Oxford University*.

Orrell, D. [2002] "Role of the metric in forecast error growth: how chaotic is the weather?," *Tellus* **54A**, 350-362.

Orrell, D., Turner, J., Giavonnoni, P., Kircher, F., Lyraud, C., Perot, J., Rifflet, J.M. & Vedrine, P. [1994] "Mechanical, thermal and electromagnetic design for a superconducting quadrupole for the SSC," *IEEE Transactions on Magnetics* **30**, 1954-1957.

Orrell, D., Smith, L.A., Barkmeijer, J., & Palmer, T. [2001] "Model error in weather forecasting," *Nonlin. Proc. Geo.* **8**, 357-371.

Figure Captions

Fig. 1. Plots of x_1 versus time, x_2 versus x_1 and log (base 10) power spectra versus frequency for various values of F for System I with $n = 4$.

Fig. 2. Bifurcation diagram for System I with $n = 4$. Upper panel is a density plot of x_1, middle panel is density of local max/min, and lower panel shows the spectral bifurcation diagram, as introduced in the text.

Fig. 3. Bifurcation diagrams for System I with $n = 8$. Upper panel is the x_1 density plot, middle panel is the density of local max/min, lower panel is the spectral bifurcation diagram.

Fig. 4. Period doubled orbit at $F = 3$ for System I with $n = 8$.

Fig. 5. Periodic orbit at $F = 5.235298$ for System I with $n = 8$.

Fig. 6. Close up of spectral bifurcation diagram in region of periodic orbit, for System I with $n = 8$. Spacing of the harmonics at $F = 5.235298$ is about 0.27, corresponding to a frequency of 36.7

Fig. 7. Bifurcation diagrams for System I with $n = 40$. Upper panel is the x_1 density plot, middle panel is the density of local max/min, lower panel is the spectral bifurcation diagram.

Fig. 8. Bifurcation diagram for the 40D System II, $\tilde{x}$ variables.

Fig. 9. Bifurcation diagrams for 40D System II, $\tilde{y}$ variables.

Fig. 10. Bifurcation diagrams for 40D System II, $\tilde{y}$ variables, as a function of the coupling coeffi cient h.

Fig. 11. $\tilde{x}$ and $\tilde{y}$ orbits for true system with $F = 2$ and $c = 1.2$.

Figures

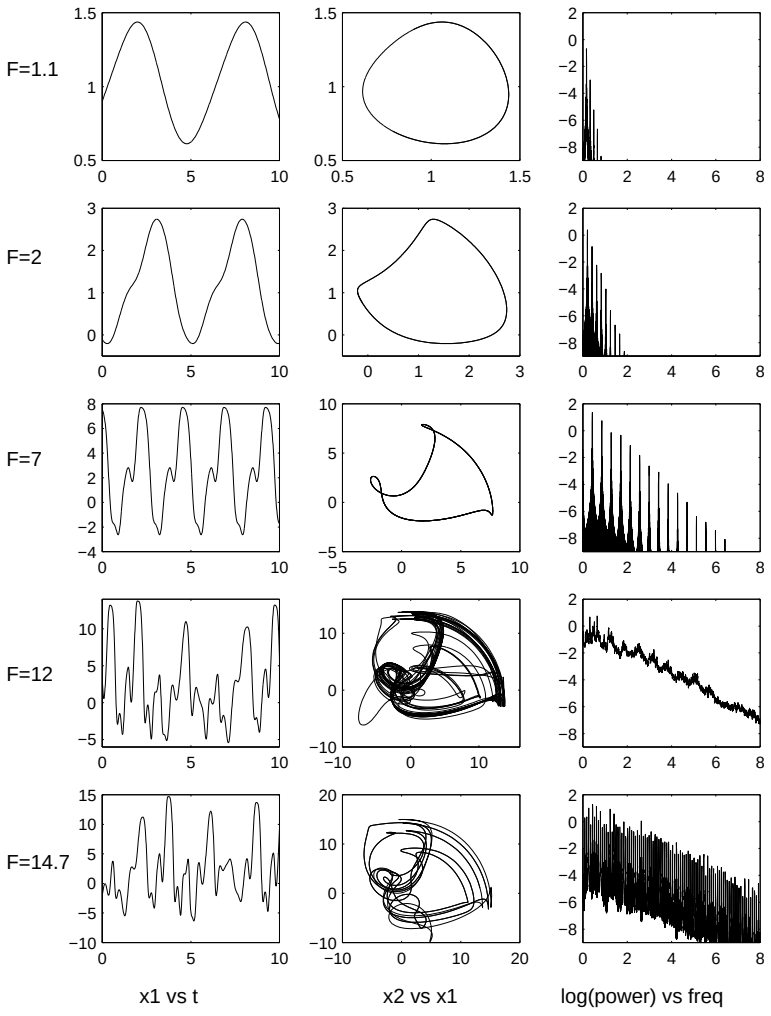

Fig. 1. Plots of x_1 versus time, x_2 versus x_1 and log (base 10) power spectra versus frequency for various values of F for System I with $n = 4$.

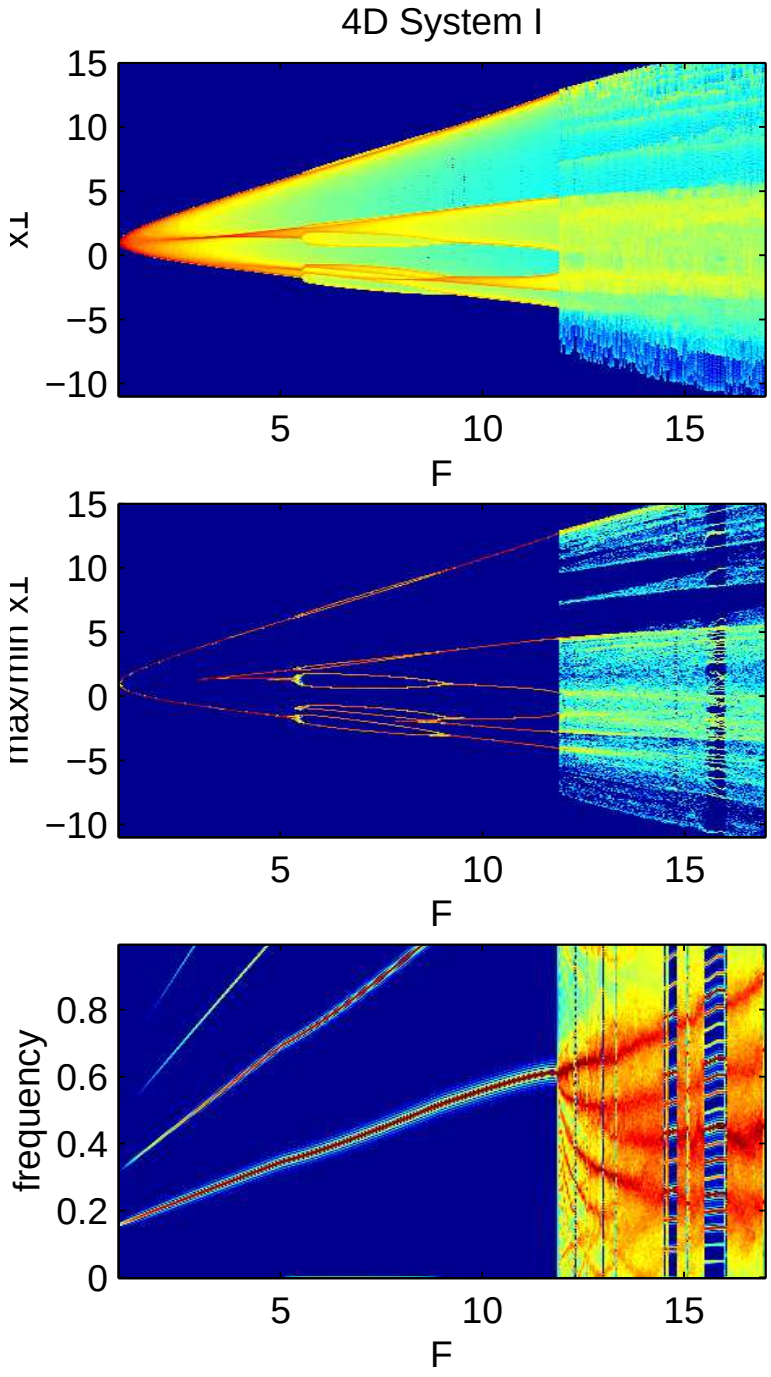

Fig. 2. Bifurcation diagram for System I with $n = 4$. Upper panel is a density plot of x_1, middle panel is density of local max/min, and lower panel shows the spectral bifurcation diagram, as introduced in the text.

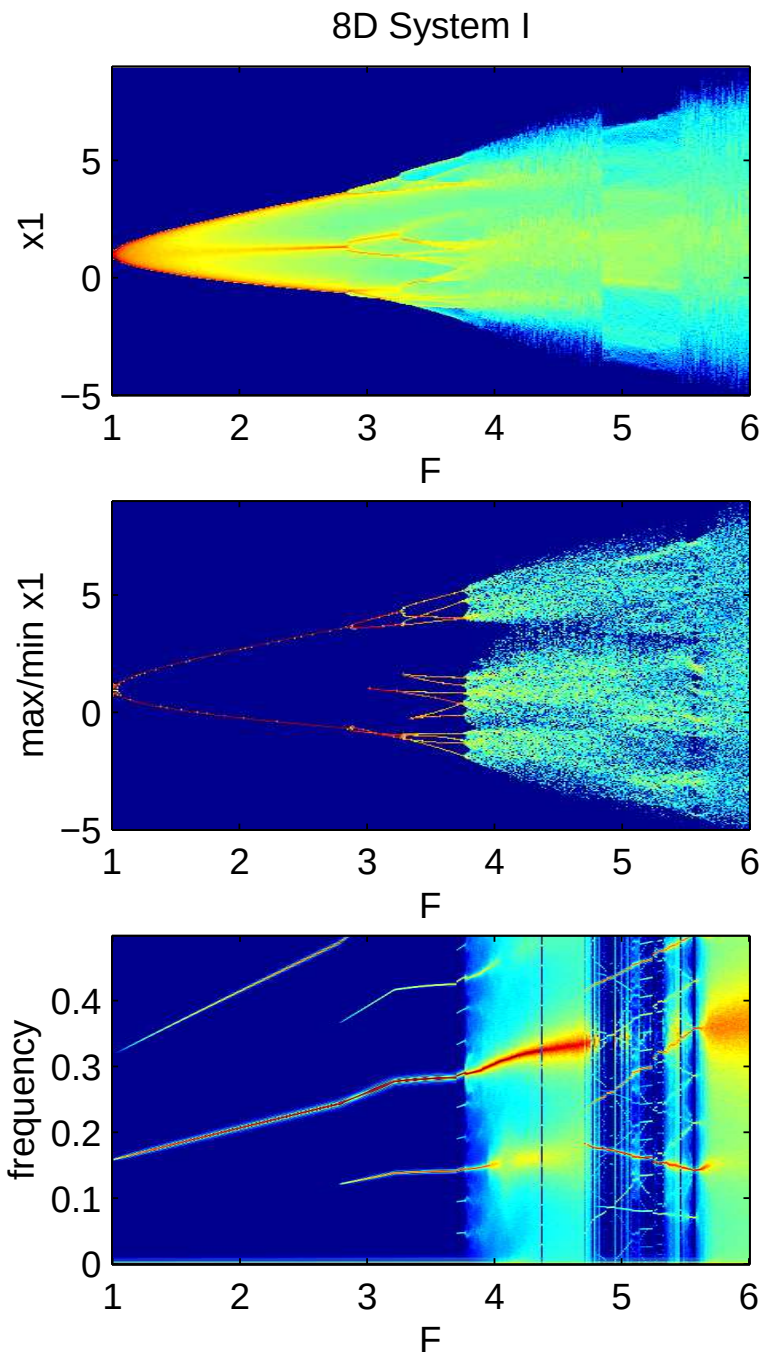

Fig. 3. Bifurcation diagrams for System I with $n = 8$. Upper panel is the x_1 density plot, middle panel is the density of local max/min, lower panel is the spectral bifurcation diagram.

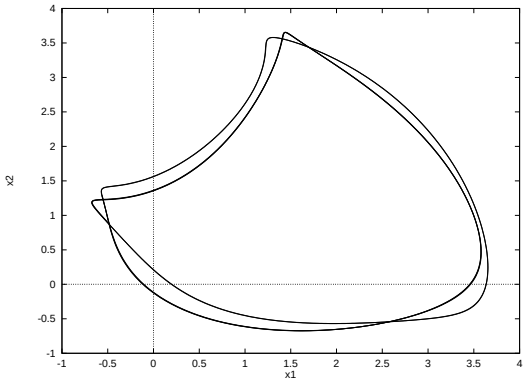

Fig. 4. Period doubled orbit at $F = 3$ for System I with $n = 8$.

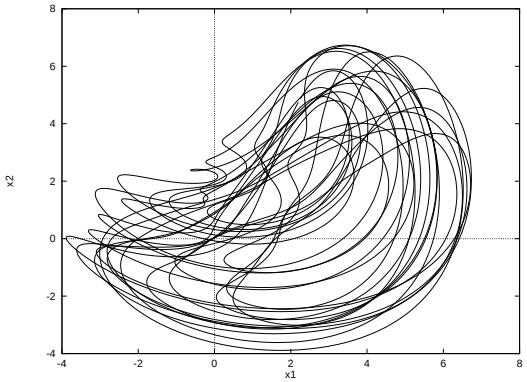

Fig. 5. Periodic orbit at $F = 5.235298$ for System I with $n = 8$.

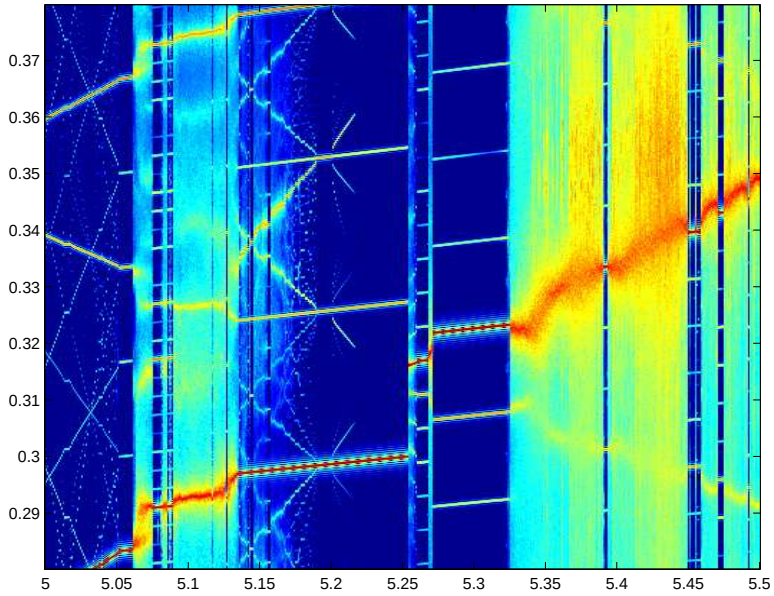

Fig. 6. Close up of spectral bifurcation diagram in region of periodic orbit, for System I with $n = 8$. Spacing of the harmonics at $F = 5.235298$ is about 0.27, corresponding to a frequency of 36.7

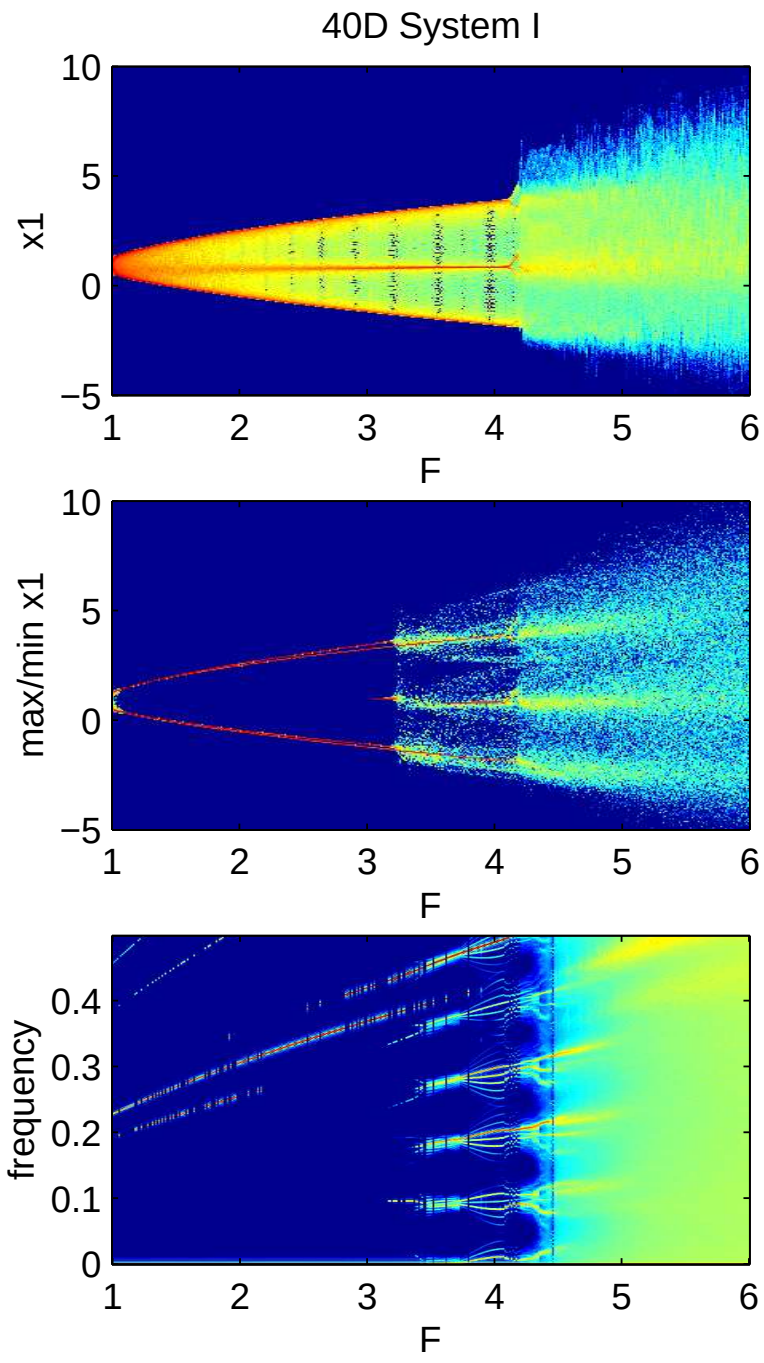

Fig. 7. Bifurcation diagrams for System I with $n = 40$. Upper panel is the x_1 density plot, middle panel is the density of local max/min, lower panel is the spectral bifurcation diagram.

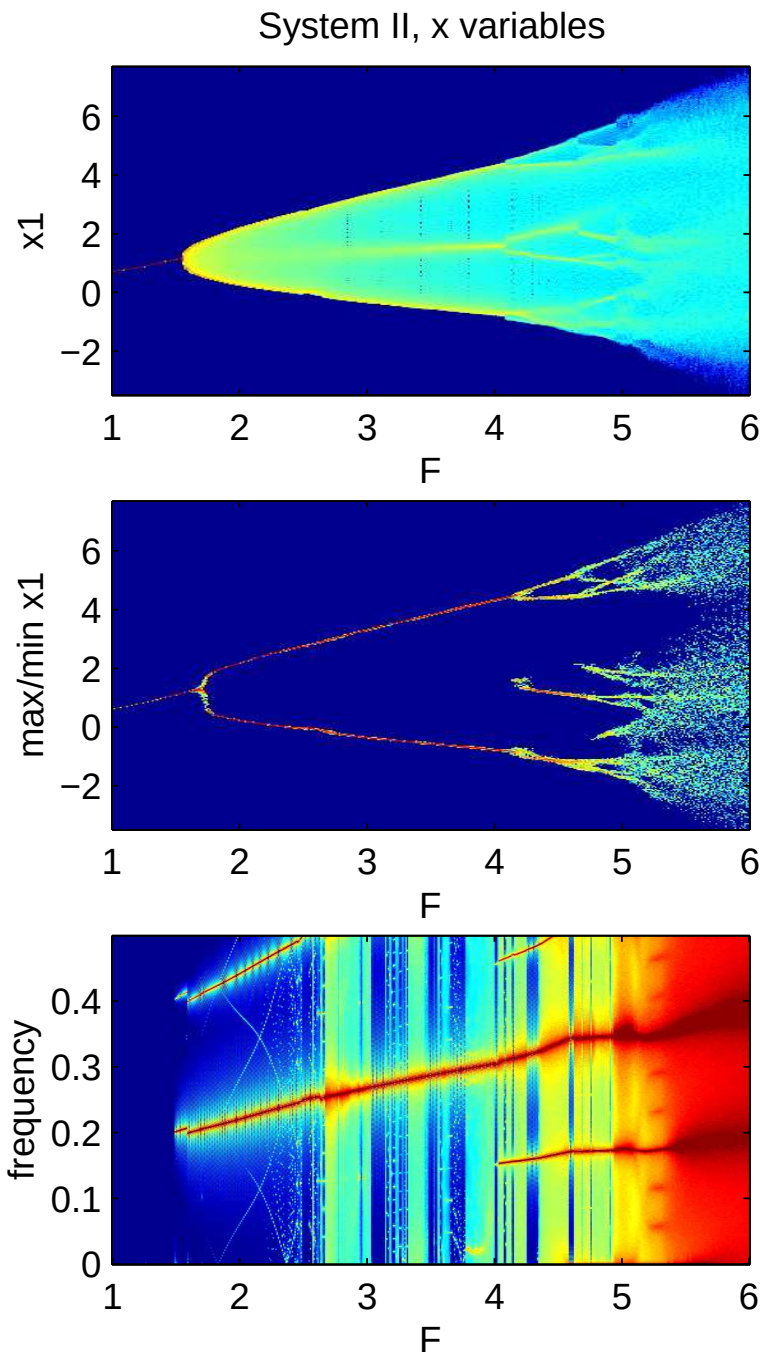

Fig. 8. Bifurcation diagram for the 40D System II, $\tilde{x}$ variables.

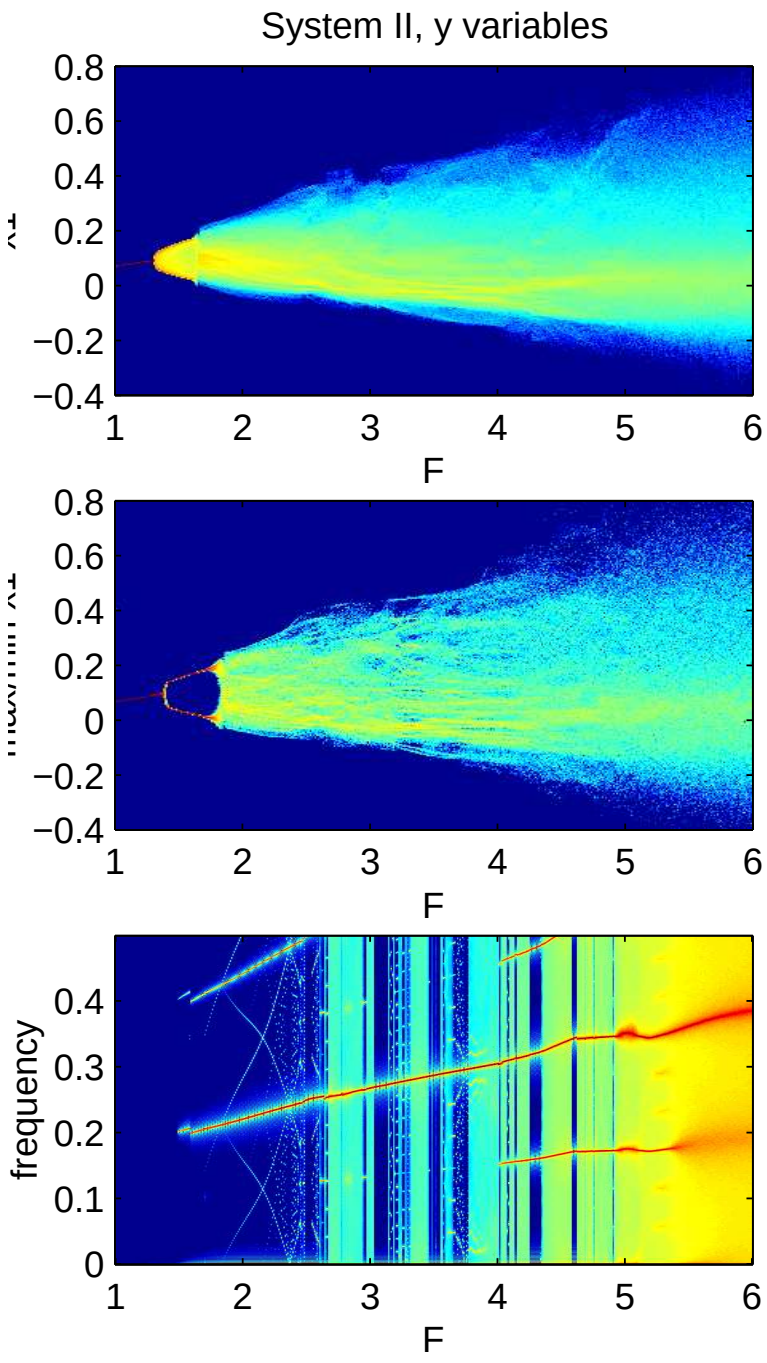

Fig. 9. Bifurcation diagrams for 40D System II, $\tilde{y}$ variables.

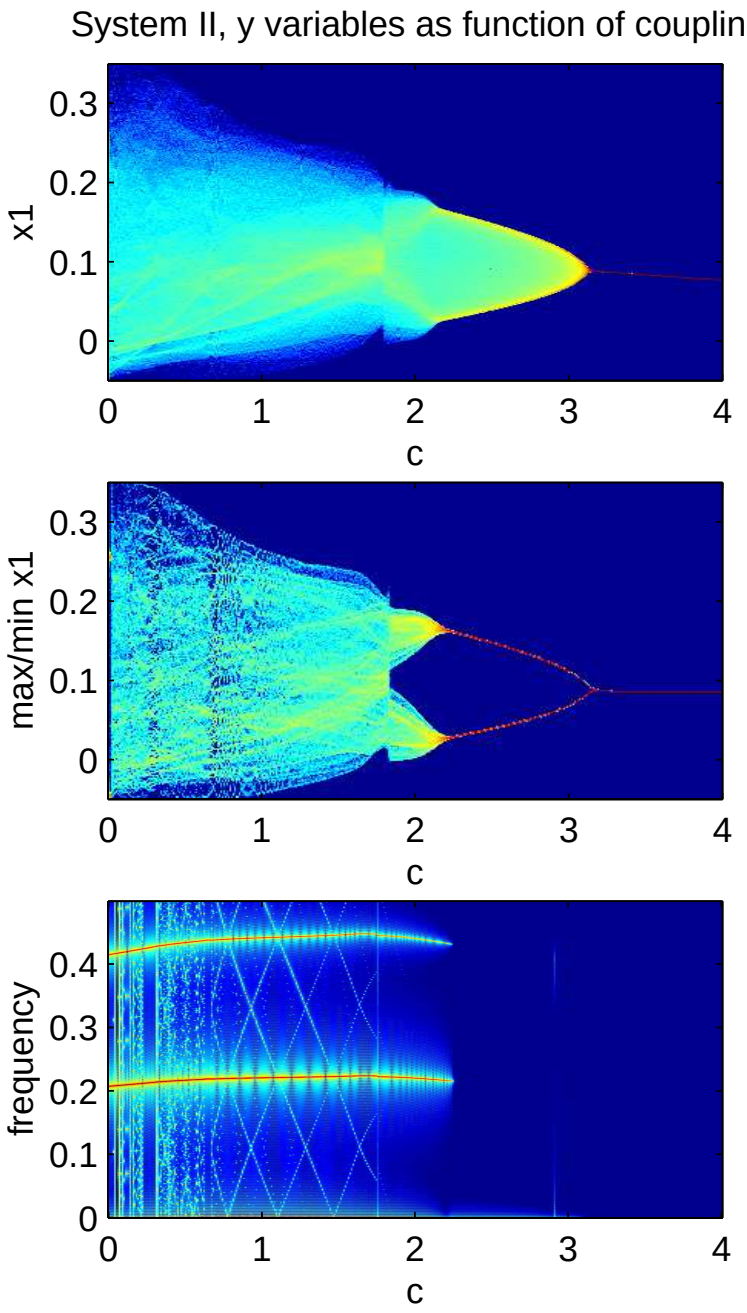

Fig. 10. Bifurcation diagrams for 40D System II, $\tilde{y}$ variables, as a function of the coupling coeffi cient h.

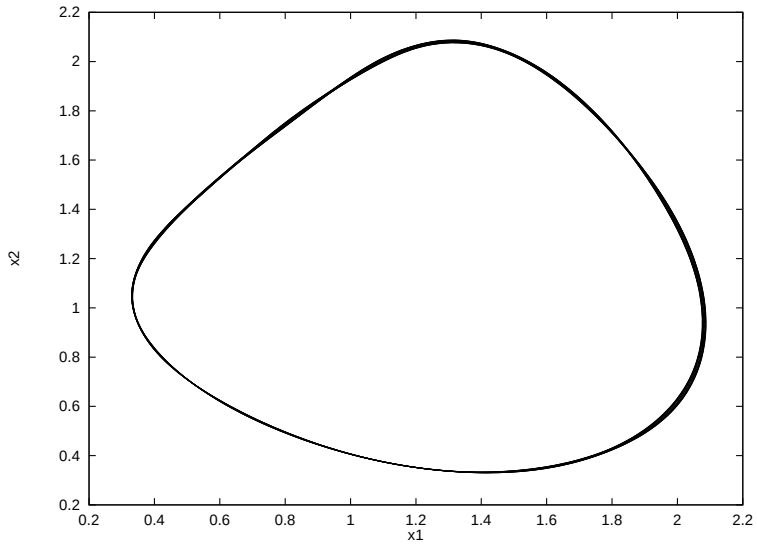

(a) $\tilde{x}_2$ versus $\tilde{x}_1$

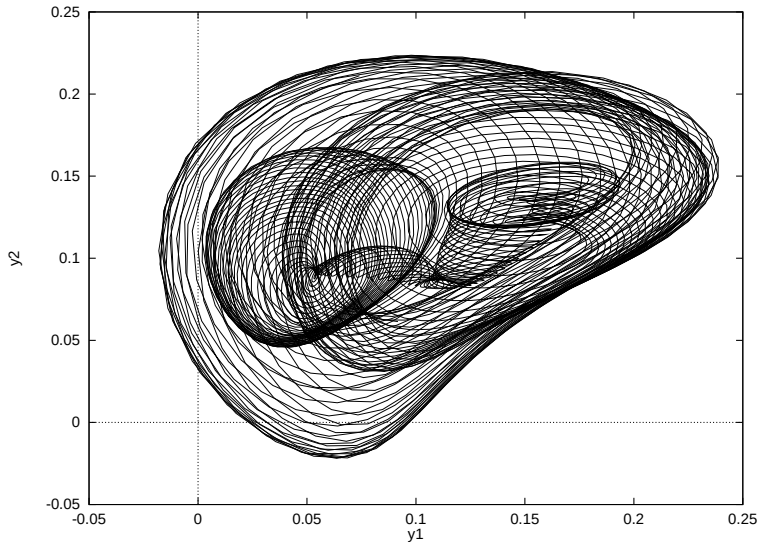

(b) $\tilde{y}_2$ versus $\tilde{y}_1$

Fig. 11. $\tilde{x}$ and $\tilde{y}$ orbits for true system with $F = 2$ and $c = 1.2$.